

Article

Low-Temperature Carburization of AL-6XN Enabled by Provisional Passivation

Zhen Li [†], Cyprian Illing , Arthur H. Heuer  and Frank Ernst ^{*,†}

Department of Materials Science and Engineering, Case Western Reserve University, 10900 Euclid Avenue, Cleveland, OH 44106, USA; zxl2191@case.edu (Z.L.); cai7@case.edu (C.I.); ahh@case.edu (A.H.H.)

* Correspondence: fxe5@case.edu; Tel.: +1-216-368-0611

† These authors contributed equally to this work.

Received: 29 September 2018; Accepted: 19 November 2018; Published: 27 November 2018

Abstract: Employing AISI-AL-6XN as example, we introduce a new method of surface activation for low-temperature carburization. This method consists of two steps: (i) removing the passivating surface oxide and a potentially existing severely plastically deformed surface layer (Beilby layer) by aqueous (liquid) hydrochloric acid, and (ii) immersion in ethanol and subsequent drying in nitrogen. Upon carburization with a gas mixture of acetylene, hydrogen, and nitrogen, this new method of surface activation enables the formation of a fully developed “case”, i.e., a uniform solid solution of interstitial carbon in austenite with carbon fractions up to 0.20 near the alloy surface. The underlying mechanism of surface activation is shown to involve the formation of a provisional passivating layer. It consists of chlorides or ethoxides that are insoluble in ethanol. It prevents the reformation of the regular Cr-rich passivating oxide layer and is readily removed upon heating and exposure to the carburizing gas. As the new activation method is quicker, more effective, and less destructive to furnace hardware than activation with hot gaseous hydrochloric acid that is currently applied in industrial manufacturing, it may have considerable technological impact.

Keywords: surface engineering; low-temperature carburization; surface activation

1. Introduction

Low-temperature carburization is a potent method of surface engineering. It can be applied to alloys that contain significant fractions of alloying elements with a high affinity for carbon. The prototype of such an alloy is the austenitic stainless steel AISI-316L (UNS designation S31603) with an atom fraction $X_{Cr} = 0.18$ of Cr as the high-carbon-affinity, carbide-forming element. The properties of finished AISI-316L alloy parts can be improved significantly by exposing them to an ambient that infuses carbon into a subsurface zone to generate a solid solution of interstitial carbon. However, owing to the high stability of Cr carbides, the equilibrium-solubility limit of carbon in this alloy is very small, corresponding to a carbon atom fraction $^{\circ}X_C \approx 10^{-6}$ at 300 K. While $^{\circ}X_C$ increases with increasing temperature, solutionizing at high temperature and subsequent quenching does not provide an easily realizable processing route: The high stability of Cr carbides substantially reduces $^{\circ}X_C$ compared to e.g., the binary system Fe–C. Even at a high temperature, $^{\circ}X_C$ is significantly smaller than the technically desired levels of e.g., $X_C \approx 0.1$. Moreover, with an increasing carbon fraction, the “C” curve of the time–temperature–transformation diagram that represents carbide precipitation moves to higher temperatures and shorter times. Therefore, (hypothetical) carburization at high temperature and subsequent quenching, unless carried out at cooling rates difficult to realize, causes the precipitation of Cr-rich carbides [1,2]. Generally, carbide formation is undesirable because it compromises important properties, especially fatigue and corrosion resistances (“sensitization”).

The desired outcome of a concentrated yet carbide-free subsurface solid solution of interstitial carbon can be obtained by carburizing at a low temperature. “Low,” in this context, means low

enough to suppress carbide precipitation by immobilizing Cr, but still high enough to enable carbon diffusion into technically useful depths within industrially feasible processing times. Idealizing these nonequilibrium conditions as a state with no metal atom mobility at all, the system is then confined to a trajectory leading to a “carbon paraequilibrium”, rather than conventional thermodynamic (or “ortho”) equilibrium [3]. With this approach, treatment times of order 0.1 Ms (1 day) can infuse carbon to an average depth $\bar{z} \approx 10 \mu\text{m}$. Within an $\approx 25 \mu\text{m}$ deep zone below the alloy surface, a carbide-free interstitial solid solution forms in which the (smoothly graded) carbon profile significantly exceeds the equilibrium solubility of carbon. At the surface, the carbon fraction can reach $X_C[0] \approx 0.15$, corresponding to $^\circ X_C \times 10^5$ at $T = 300 \text{ K}$. Similar considerations apply to the low-temperature infusion of nitrogen or a combination of nitrogen and carbon.

The interstitial solute-rich subsurface zone, denoted as a “case”, can dramatically improve the performance of alloy parts in technical applications. Typical benefits include a fourfold increase of surface hardness [4], the reduction of wear volume by a factor of order 10^2 [5], an increase in high-cycle fatigue life by a factor of order 10^2 [6], and a significant enhancement of corrosion resistance, particularly in seawater [7–9].

For industrial applications of low-temperature carburization, gas-phase processes are important, i.e., exposing alloy parts contained in a furnace to a gas that provides elemental carbon or nitrogen to diffuse into the alloy. Swagelok Company (Solon, OH, USA) invented a low-temperature atmospheric pressure gas-phase carburization process for AISI-316L stainless steel [4,10,11]. However, for alloys with a Cr fraction suitably high for low-temperature carburization (or nitridation or nitro-carburization), successful carburization from a gas phase first requires surface “activation”: The surface of AISI-316L and related “stainless” alloys is typically covered by a $\approx 1 \text{ nm}$ thick Cr-rich oxide layer [12] that (i) passivates the alloy against low-temperature corrosion and (ii) constitutes a diffusion barrier to carbon and nitrogen (Figure 1).



Figure 1. Schematic cross-section of alloy architecture before low-temperature carburization. (Core: alloy core with bulk properties. BL: Beilby layer. PL: Passivating Cr-rich oxide layer.

Another potential obstacle to carbon or nitrogen infusion into alloy parts can originate from machining-induced severe plastic deformation, poor crystallinity, and contamination in a zone directly below the surface, known as the “Beilby” layer (Figure 1) [13]. This has been confirmed by the results of Ge et al. [14,15] on acetylene-based low-temperature carburization of AISI-316L.

Our current understanding is that the passivating oxide layer must be removed before carbon or nitrogen can diffuse into the alloy. Removal of the Beilby layer may not be critical, but can boost the efficacy of low-temperature carburization/nitridation/nitrocarburization. Accordingly, both layers should be removed prior to the infusion of interstitial solute. An established method for such “surface activation”, i.e., removing the passivating oxide layer and potentially the Beilby layer, is the application of hot gaseous HCl (hydrochloric acid). For example, the low-temperature carburization process established by Swagelok uses gaseous HCl at 520 K directly before the infusion of interstitial solute [4]. However, it was empirically found that a single in situ exposure to gaseous HCl does not sufficiently activate the surface of AISI-316L. Activation by gaseous HCl is substantially more effective after some carbon has already been infused into the specimen. For this reason, the Swagelok process operates with “double activation”, consisting of two subsequent gaseous HCl activation steps interlaced with an initial step of low-temperature carburization [4,11]. The total time for activation is 32 ks (9 h), one-third to one-half the low-temperature carburization time of 0.1 Ms (20 to 30 h). Moreover, gaseous HCl is aggressive and can damage non-corrosion-resistant processing furnace hardware.

In this article, we report the discovery that the industrially established in situ surface activation process using gaseous HCl can effectively be replaced by the following ex situ procedure: (i) immersing the alloy part in a liquid etchant (concentrated aqueous HCl) at room temperature, (ii) stopping the etch process by directly transferring the specimen into a reservoir of C₂H₅OH (without prior drying), (iii) loading the specimens into a furnace for gas-phase low-temperature carburization, purged with dry N₂ gas, (iv) and heating them and exposing them to streaming carburizing gas. In this way, alloy parts can be directly carburized by exposure to carburizing gas (C₂H₂, H₂, N₂) at 723 K without prior application of gaseous HCl. The total additional processing time for activation, Step (i) and (ii), is less than 1 ks (17 min)—one-hundredth of the low-temperature carburization time and \approx 30 times shorter than in the Swagelok process.

That low-temperature carburization can be successfully carried out directly after ex situ etching and cleaning/storing leads to the hypothesis that the specific cleaning/storing procedure we are applying inhibits the spontaneous reformation of the regular passivating oxide layer. Instead, this procedure seems to provide “provisional” passivation that inhibits the formation of the usual Cr-rich passivating oxide film and is readily removed when the alloy is subjected to low-temperature carburization, by the applied temperature or by reaction with the carburizing gas.

The alloy for which we demonstrate the efficacy of “provisional passivation” is AISI-AL-6XN (UNS designation N08367, Table 1), a superaustenitic stainless steel containing higher fractions of Ni and Mo than AISI-316L. Enhanced fractions of Ni and Mo provide superaustenitic stainless steels with better corrosion resistance than martensitic-, ferritic-, and 300-series austenitic stainless steels. At the same time, they have higher strength than austenitic steels AISI-304 (UNS designation S30403) and AISI-316, making them attractive for demanding applications. Additionally, superaustenitic stainless steels have excellent strength and oxidation resistance at elevated temperatures [16]. The hardness of AISI-AL-6XN, on the other hand, is not significantly higher than that of e.g., AISI-304 and AISI-316 [8]. The lack of higher hardness is particularly limiting in applications demanding high wear resistance. Previous work has demonstrated that the surface hardness of AISI-AL-6XN can be significantly improved by low-temperature carburization [17] while not compromising their excellent corrosion resistance [18]. Therefore, low-temperature carburization provides potential for expanding the range of technical applications in which AISI-AL-6XN can serve.

Table 1. Composition of AISI-AL-6XN.

Element	Fe	Ni	Cr	Mo	Mn	Si	C
Atom Fraction	0.4308	0.2461	0.2396	0.0413	0.0206	0.0202	0.0014

2. Experimental Methods

To explore the possibility of removing the passivating oxide layer ex situ and the effect of the Beilby layer on the efficacy of low-temperature carburization, we carburized a series of AISI-AL-6XN specimens prepared without and with severely plastically deformed surface layers of different depth. Specimens without (or minimal) Beilby layer were prepared by electropolishing. Specimens with Beilby layers of different depth were prepared by polishing to three different surface finishes using water-cooled SiC paper with grade: (i) P180, (ii) P800, and (iii) P4000. With each one of these four different surface preparations, these samples were further prepared for low-temperature carburization by (i) etching in concentrated, ($12 \text{ kmol}\cdot\text{m}^{-3} = 12 \text{ M}$) aqueous HCl (liquid hydrochloric acid) at room temperature for $\tau_1 = 0.60 \text{ ks}$ (10 min), (ii) transferring the HCl-covered specimens directly, without washing or drying, into a reservoir of nominally pure C₂H₅OH. Corresponding control samples were not etched in HCl, just directly stored in C₂H₅OH. Owing to the size of the C₂H₅OH reservoir compared to the specimen surface area, the amount of HCl carried into the C₂H₅OH with the specimen is estimated to a molar fraction $<5 \times 10^{-3}$. The specimens remained in the C₂H₅OH reservoir for $\tau_2 = 0.3 \text{ ks}$ (5 min). Then, within $\tau_3 = 0.03 \text{ ks}$, without letting the C₂H₅OH completely evaporate off

the alloy surface, the specimens were transferred into the carburization furnace, purged with dry N_2 gas. Immediately after transfer into the furnace, the specimens were heated and low-temperature carburization was carried out at 723 K for 72 ks (20 h) in a streaming gas mixture containing C_2H_2 (acetylene), N_2 , and H_2 with volume ratios of 1:50:3. (The time and temperature were chosen equivalent to the process established by Swagelok [4]).

For metallographic work after low-temperature carburization, cross-sectional specimens were polished to mirror finish. Their microstructure was developed by etching for 90 s, with a few drops of a reagent consisting of concentrated aqueous HCl, concentrated aqueous HNO_3 ($16 \text{ kmol}\cdot\text{m}^{-3} = 16 \text{ M}$), and H_2O with volume ratios of 2:1:1. Light-optical images revealing the microstructure were obtained from these specimens using an Olympus FV1000 Laser Scanning Confocal Microscope (Olympus, Center Valley, PA, USA).

For X-ray diffractometry, we employed a Bruker Discover D8 X-ray diffractometer (Bruker Corporation, Billerica, MA, USA) equipped with a monochromated $Co-K_{\alpha}$ X-ray source.

Cross-sectional atom-fraction–depth profiles (hereafter abbreviated as “profiles”) were measured by a Physical Electronics PHI-680 scanning Auger microprobe (Physical Electronics, Chanhassen, MN, USA), after calibration using specimens of Fe and Fe carbides and nitrides with known compositions. The instrument was set up to collect signals from Fe, Cr, Ni, Nb, Mo, carbon, and oxygen. Carbon profiles determined by scanning Auger microprobe tend to suffer from noise. Owing to the differentiation that is carried out during signal processing, this produces a background that varies dependent on the signal level and is particularly strong in regions of low signal (e.g., in carbon profiles acquired from regions of low carbon fraction). To subtract the background, we applied a method recently developed for this purpose [19]. As a result of removing the background, but not the noise, the resulting discrete carbon profile exhibits partly negative X_C in low-carbon regions where the noise exceeds the average carbon level.

3. Results

Figure 2 presents cross-sectional light-optical microscopy images of all samples at the same magnification. The left column contains the micrographs from specimens that were activated by etching in aqueous HCl, whereas the right column shows micrographs from specimens prepared without activation. Micrographs in the same row are from specimens with the same mechanical surface preparation. The two micrographs in the top row are from electropolished samples, followed by samples ground by SiC paper with increasing coarseness (P4000, P800, P180).

All micrographs reveal similar grain structures in the alloy core, i.e., in depths to which no significant amounts of carbon could diffuse within the low-temperature carburization processing time. (Differences in appearance are merely the result of under- or overetching.) While a Beilby layer introduced by surface machining typically involves a subsurface zone of reduced grain size, this is not observed here: Regarding grain morphology, the zone directly below the surface appears to be no different from the alloy core. Some of the micrographs exhibit a bright band below the surface, or fragments thereof (Figure 2d,f). This indicates the formation of a “case”, i.e., a zone with a carbon fraction X_C high enough to provide corrosion resistance against the metallographic etchant, preventing it from developing the grain structure. However, what appears to be a uniform layer with a sharp boundary to the alloy core does not properly reflect the properties of the underlying carbon profile, which is actually smoothly graded, as expected for a diffusion profile (see scanning Auger microprobe data below). Rather, the apparently sharp border between the case and the core indicates that a critical level of carbon is required to make the alloy resistant against the metallographic etchant and a surface step develops in this region as a result of local galvanic element formation. Nevertheless, comparing the apparent thickness of the nonetched case layer in micrographs obtained with the same procedure of metallographic etching provides a useful (monotonic relative) measure for the level of carbon uptake and penetration during low-temperature carburization.

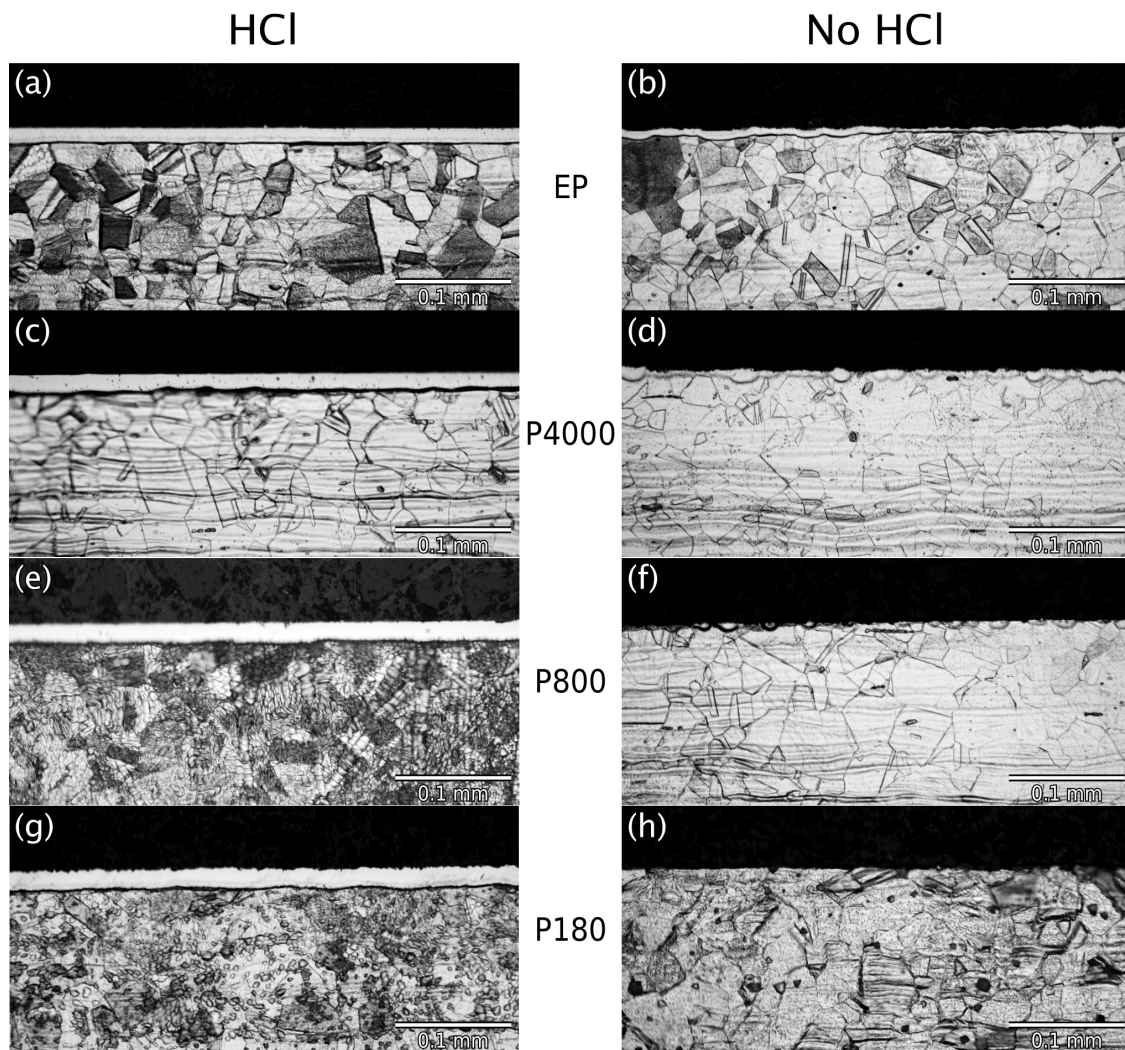


Figure 2. Cross-sectional light-optical microscopy of low-temperature-carburized AISI-AL-6XN, obtained with the following combinations of mechanical pre-preparation and chemical etching. (a) Electropolished, HCl. (b) Electropolished, not etched. (c) P4000, HCl. (d) P4000, not etched. (e) P800, HCl. (f) P800, not etched. (g) P180, HCl. (h) P180, not etched.

Figure 2 provides the following important results: Regardless of Beilby layer depth, all samples etched in HCl developed a continuous case (carbon-rich layer) with excellent thickness uniformity. Figure 2a,c,e,g consistently exhibits an apparent average case thickness of 0.02 mm. This means that etching in aqueous HCl has properly removed the passivating oxide layer, regardless of Beilby layer thickness.

In the micrographs in the right column of Figure 2, a continuous case is only observed for the electropolished specimen. While significantly thinner than the case thickness obtained with HCl etching (left column), this observation shows some ability of the carburizing gas itself to activate the surface by removing the passivating oxide layer. The average apparent case thickness is only about 1/3 of the case thickness observed after HCl etching. Additionally, the case thickness seen in Figure 2b exhibits strong local variations, indicating that the activation is slow and locally incomplete.

The nonetched specimens prepared with a Beilby layer (Figure 2d,f,h) exhibit no continuous case at all. Figure 2d (P4000) features semiglobular fragments of a case, apparently growing in from the surface. In Figure 2f (P800), similar features appear, but are even less developed. Figure 2h (P180), obtained from the specimen with the thickest Beilby layer, does not exhibit any trace of case formation. These observations demonstrate that both the passivating oxide and the Beilby layer

can be similarly effective diffusion barriers to carbon infusion at low temperature: The inhibiting effect of the passivating oxide layer follows from the fact that the carbon penetration of the electropolished nonetched sample is less than for the HCl-etched samples (assuming that the oxide layer that forms during or after electropolishing is equivalent to the passivating oxide layer that “normally” forms on AISI-AL-6XN). The inhibiting effect of the Beilby layer follows from the decrease of carbon penetration with increasing Beilby layer thickness.

Given that the Beilby layer constitutes an effective carbon-diffusion barrier, the fact that the apparent case thickness in the left column of Figure 2 does not significantly differ between specimens with different mechanical pre-preparation indicates that the severely plastically deformed subsurface zone generated by the respective procedures (electropolishing, mechanical grinding) has been completely etched away by the application of aqueous HCl.

The efficacy of activation by aqueous HCl is further demonstrated by X-ray diffractometry and scanning Auger microprobe carbon-fraction–depth profiling. Figure 3 shows a comparison between the X-ray diffractogram of low-temperature carburization AISI-AL-6XN, activated with HCl, and non-carburized AISI-AL-6XN. The 111 and 200 peak positions of nontreated AISI-AL-6XN are consistent with the anticipated lattice parameter of 0.36 nm. The peaks are sharp and there are no (e.g., carbide) peaks in addition to those expected from austenite.

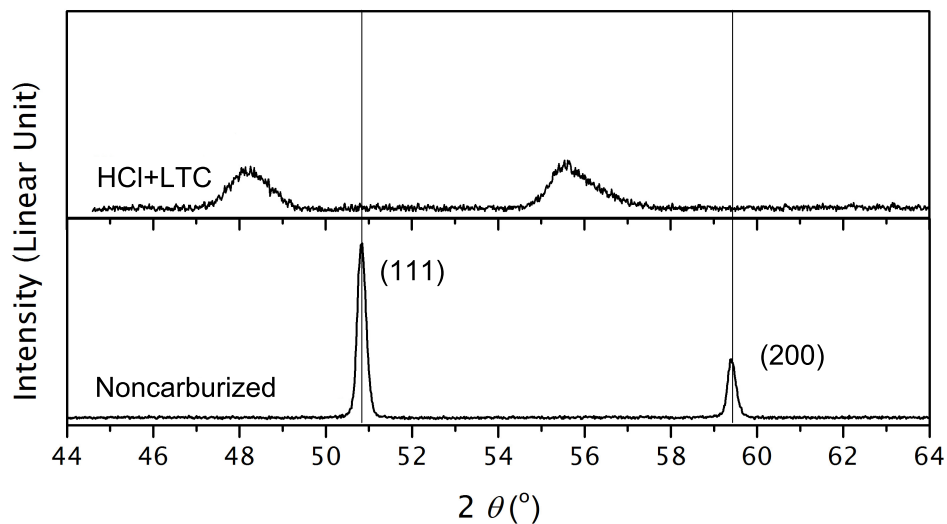


Figure 3. X-ray diffractogram of noncarburized and carburized AISI-AL-6XN.

After low-temperature carburization with HCl activation, the corresponding peaks are shifted to lower diffraction angles, indicating increased interatomic distances between the metal atoms. The peak shift is almost twice the peak shift observed for AISI-316L reported in Reference [4], consistent with the maximum carbon fraction also being almost twice as large. The peaks are also broadened. This can be attributed to two effects: (i) As the carbon profile is graded, the peak shape corresponds to a weighed average over lattice plane spacings that decrease with increasing depth below the alloy surface. (ii) A high dislocation density caused by stress that builds up between the region of expanded interatomic distances at the surface and the noncarburized alloy core [20].

Figure 4 shows a carbon profile measured on the cross-sectional AISI-AL-6XN specimen by scanning Auger microprobe. Defining the case depth as the depth at which the signal vanishes in the background noise, the case depth is $\approx 20 \mu\text{m}$, which is comparable to the case depth suggested by the metallographic images in Figure 2. As expected, the maximum carbon fraction is observed at the surface: $X_C[0] = 0.2$. The carbon profile gradually decreases with increasing z , exhibiting a concave shape characteristic of a diffusion coefficient that increases with increasing X_C [21].

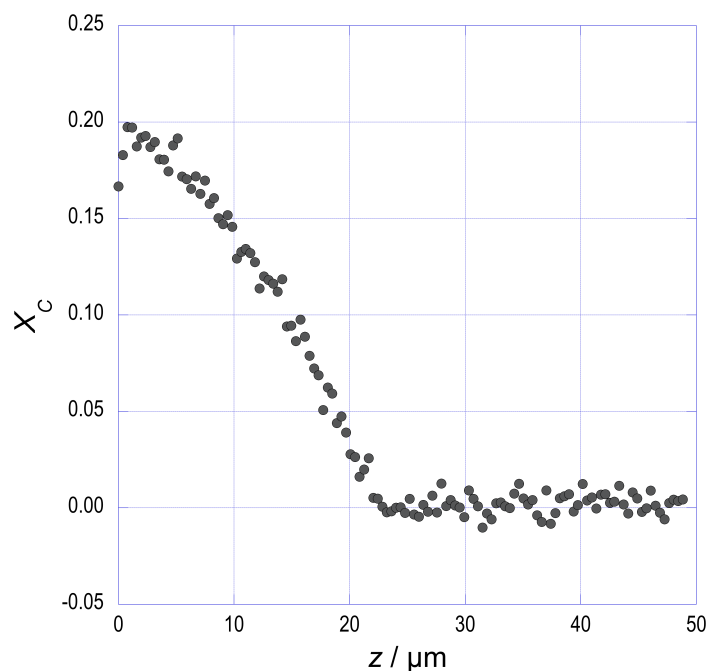


Figure 4. Atom-fraction–depth profile $X_C[z]$ of carbon in low-temperature-carburized AISI-AL-6XN, acquired by scanning Auger microprobe. The alloy was activated by etching in concentrated aqueous HCl, immersing in C_2H_5OH , and drying in N_2 .

Comparison of Figure 4 and the apparent case thickness observed in the left column of Figure 2 shows that a carbon fraction $X_C > 0.05$ is needed to establish corrosion resistance against the metallographic etchant.

While Figure 2 indicates the “case depth” (i.e., depth of the zone where $X_C > 0.05$), the carbon profile of Figure 4 and the magnitude of the peak shift observed in Figure 3 prove that the case actually has the expected high level of carbon. Further, Figure 3 proves that the volume fraction of potentially existing additional phases (carbides) is below the volume fraction that X-ray diffractometry can detect, estimated as 0.05.

4. Discussion

The empirically developed surface activation by HCl gas that is part of the Swagelok (industrial) low-temperature carburization process is carried out at 520 K ($250^\circ C$) for 7.2 ks (3 h), and it is carried out twice with a 743 K ($470^\circ C$) 7.2 ks (3 h) low-temperature carburization step in between. Room-temperature etching in aqueous HCl for 0.6 ks (10 min) and immersing in C_2H_5OH for 0.5 ks (5 min) is a much more effective way of surface activation. The efficacy of aqueous HCl in removing the passivating oxide layer and Beilby layer, compared to gaseous HCl, can be rationalized by the 10^3 times higher density of aqueous HCl.

The experimental observations can be understood in terms of the model shown in Figure 5: Generally, as-received AISI-AL-6XN exhibits a passivating oxide layer at the surface and a Beilby layer in the zone below. Typically, this includes a zone of nanosized grains or subgrains directly below the surface [14], as well as an increased density of line and point defects. Contrary to what the terminology suggests (“Beilby layer”), this layer has no well-defined thickness. Rather, the number-density–depth profiles of the defects that characterize the Beilby layer are smoothly graded, i.e., a steady function of depth z , and the profiles of different defect species fall off differently with increasing z .

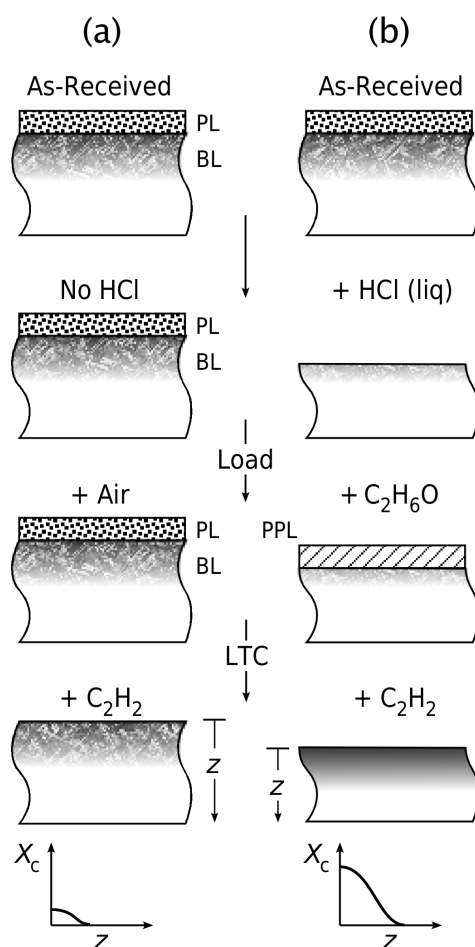


Figure 5. Schematic showing the structuring of AISI-AL-6XN in various stages. (a) Direct low-temperature carburization of the as-received alloy, featuring a passivating oxide layer and a Beilby layer. C_2H_2 (acetylene), the carburizing gas, removes the passivating oxide layer, but does not etch the alloy. The Beilby layer acts as a carbon diffusion barrier, resulting in an underdeveloped (or nonexistent) carbon-fraction–depth profile $X_C[z]$. (b) Etching in concentrated aqueous HCl removes the passivating oxide layer and the Beilby layer. Storing in C_2H_5OH and drying in N_2 (on moving into the gas furnace) results in a provisional passivating layer. Low-temperature carburization with C_2H_2 readily removes the provisional passivating layer to generate a fully-developed $X_C[z]$.

Figure 5a illustrates the process without external activation: If no HCl (or other etching) is applied, and the material is exposed directly to low-temperature carburization, an underdeveloped carbon profile results, or none at all ($X_C[z] = 0$). This is because of two reasons: (i) While C_2H_2 can activate the surface by removing the passivating oxide layer, it does not remove the passivating oxide layer as efficiently as e.g., gaseous HCl. (ii) C_2H_2 does not etch the alloy. Therefore, a potentially existing Beilby layer is not removed and remains as a diffusion barrier to carbon.

Figure 5b shows the corresponding stages with external activation: External etching in concentrated aqueous HCl removes the passivating oxide layer and the Beilby layer—or at least the (presumably uppermost) subzone of the Beilby layer that inhibits carbon diffusion. Storing in C_2H_5OH results in a provisional passivating layer. This provisional layer protects the alloy surface against the reformation of the Cr-rich passivating oxide film. At the beginning of the low-temperature carburization process, the increasing temperature and interaction with C_2H_2 readily remove the provisional passivating layer, exposing a fully activated surface to the carburizing gas. This results in a fully-developed carbon profile.

Our results and the model of Figure 5 are consistent with the findings of Somers et al. [22], who reported that C_2H_2 has the ability to activate and carburize Fe–Cr–Ni alloys. The work of Ge et al. [14] confirmed that C_2H_2 can carburize AISI-316L at low temperatures, but only if a potentially existing Beilby layer introduced by machining was first polished off. AISI-316L specimens with a coarse surface finish did not carburize well. These observations indicated that C_2H_2 can remove the passivating oxide layer, but does not etch the alloy and therefore cannot remove the Beilby layer.

The detailed mechanisms by which the Beilby layer, i.e., a severely plastically deformed layer, inhibits the diffusion of interstitially dissolved carbon, are complex and currently not understood. It is known, however, the Beilby layer contains high dislocation density. Owing to locally increased free volume, dislocations can accelerate the diffusion of interstitial atoms (although the concept of “pipe” diffusion may not apply [23]). On the other hand, the interaction of the stress fields caused by dislocations and interstitial atoms causes dislocations to bind carbon atoms in “Cottrell clouds” [24]. Quantitatively, simulations (for the body-centered cubic structure) suggest that, for 70% of the total time, carbon atoms diffuse within a distance of ≤ 1 nm from the dislocation core [25]. This effectively reduces the normally three-dimensional diffusion to one-dimensional diffusion along the dislocation line. Moreover, the carbon fraction within the Cottrell clouds is higher than in dislocation-free regions. For the high carbon fractions considered here in the context of low-temperature carburization, the enhanced X_C in Cottrell clouds may lead to a configuration in which the availability of free interstitial sites to jump into becomes limiting for diffusivity. This effect has been observed earlier by Christiansen et al. in experiments revealing the concentration dependence of the nitrogen-diffusion coefficient in AISI-304 and AISI-316 [26]. Reduced availability of vacant interstitial sites combined with the reduced dimensionality of diffusion explains why austenite regions with high dislocation density act as a carbon diffusion barrier, rather than enhancing diffusion.

Another effect of the Beilby layer may arise from the fact that it is likely to contain passivating oxide layer fragments that initially formed on the alloy surface in contact with air and were kneaded into the Beilby layer that formed during subsequent machining. In earlier work, we concluded that the oxide particles can retard or prevent the ingress of carbon [14].

The formation of a provisional passivating layer on or after immersion in C_2H_5OH is a compelling hypothesis: The bare metal surface is not stable in air. On the other hand, the formation of the regular passivating layer is known to inhibit low-temperature carburization. This means that a passivating film must form, but it is not the usual Cr-rich oxide film. The observed phenomenon resembles the provisional passivation of Si {100} surface with aqueous HF solution, which is common in semiconductor technology [27,28]. In that case, dangling bonds of Si are saturated by a monolayer of hydrogen, preventing the formation of the usual passivating SiO_2 layer. Different from a SiO_2 layer, the provisional passivating layer formed by hydrogen readily desorbs upon heating to expose a pristine Si surface, e.g., for epitaxy.

Previous work [17,29] demonstrated that aqueous HCl can also effectively activate AISI-316L for low-temperature carburization. Comparative experiments in which the etching by aqueous HCl was followed by rinsing in C_2H_5OH in one case and rinsing in H_2O in the other case demonstrated that immersion in H_2O after aqueous HCl etching does not enable subsequent low-temperature carburization, and, thus, does not accomplish provisional passivation.

Based on these observations, we now discuss three alternative hypotheses for the mechanism of provisional passivation of the alloy in the period between removing the passivating oxide layer by aqueous HCl and the beginning of carbon infusion.

1. Provisional passivation by liquid ethanol. In principle, it is possible to protect a bare metal surface against oxidation by an oxygen-free liquid. As described under “Experimental Methods”, the specimens were covered by liquid ethanol for the entire period between HCl etching and drying in streaming dry N_2 in the carburization furnace. This could explain the success of our procedure if covering the alloy surface with ethanol were sufficient to reduce contact with oxygen to a level at which reformation of the passivating oxide layer is impossible within the given amount of time.

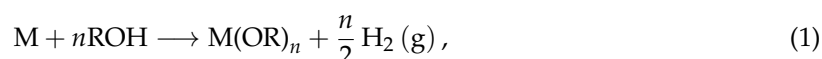
However, the literature data on the solubility and diffusivity of oxygen in ethanol do not support this hypothesis.

Based on the literature data [30], nominally pure C₂H₅OH at room temperature (293 K) can contain dissolved oxygen up to a mole fraction of 6×10^{-4} . This means that an C₂H₅OH layer with a thickness of 2 μm contains enough oxygen to build up the regular passivating oxide layer with its thickness of 1 nm. In C₂H₅OH–C₆H₅CH₃ solution at room temperature, the diffusion coefficient of oxygen is $D_O = 5 \times 10^{-9} \text{ m}^2 \cdot \text{s}^{-1}$ [31]. Assuming the same diffusivity for oxygen in C₂H₅OH implies that within the $\tau_2 = 0.3 \text{ ks}$ (5 min) for which the specimens are stored in C₂H₅OH, the typical diffusion distance $\bar{x}_1 \approx \sqrt{D_O \tau_2} = 1 \text{ mm}$. Thus, the diffusion distance is about 500 times larger than the thickness of the C₂H₅OH layer that could provide enough oxygen to build up a regular passivating oxide layer. Ergo, the observation that a regular passivating oxide layer does not reform while the specimens are stored under C₂H₅OH cannot be explained by a lack of oxygen.

Within the $\tau_3 = 0.03 \text{ ks}$ of transferring the specimens into the furnace, the diffusion distance $\bar{x}_2 \approx \sqrt{D_O \tau_3} = 0.4 \text{ mm}$. As the C₂H₅OH film on the specimens becomes thinner than \bar{x}_2 , oxygen from the ambient air can reach the metal surface to form a regular passivating oxide layer. Summarizing, it seems unlikely that the effect of C₂H₅OH is simply to “seal” the metal surface against contact with oxygen.

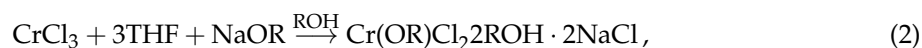
2. Provisional passivation by ethoxides. Here, the hypothesis is that contact of the HCl-etched bare metal surface with C₂H₅OH causes the formation of a provisional passivating layer consisting of ethoxides. As the pyrolysis temperature of metal ethoxide can be as low as 520 K [32], they may readily pyrolyze during heating for low-temperature carburization, leaving oxides of all involved metals on the surface [32–34]. It is known that Fe and Ni oxides are transparent to the infusion of carbon at low temperature [35]. However, a detailed analysis, sketched in the following, does not support this model:

The conjugate base of an alcohol (R–OH) is the alkoxide ion (RO[−]). Typically, alkoxides readily form ligands, act as strong bases, and are nucleophilic when they have nonbulky R-groups [36]. Metal alkoxides can be monomeric or polymeric and can form complex macromolecules [33,36–38]. Highly electropositive metals may react directly with an alcohol solution, leading to the formation of an alkoxide [36]. Such reactions may dissolve metal in the alcohol, forming hydrogen gas and an insoluble alkoxide, following the general reaction:



where the alcohol may be methanol, ethanol, etc. However, this route is unlikely for transition-metal alkoxide formation [36].

For some transition-metal alkoxides, a metal–halide feed stock reacts with sodium alkoxides in an alcohol solution. A metathesis reaction (mutual ion exchange) occurs with the precipitation of the less-soluble product [33,36,38–41]. An example is:



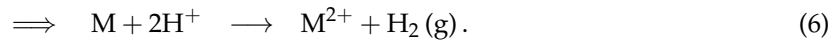
where THF is tetrahydrofuran [41].

Another route for transition-metal alkoxide formation is oxidative synthesis. Here, H–OR additions are made to the metal centers of ligands. α -ligand metathesis reactions are such a pathway [37]. They only involve one metal, more credible as an avenue for the formation of a provisional passivating layer. An example reaction is:



where only hydrogen atoms are exchanged between α -ligands [37]. However, these reactions are not likely to readily proceed with the transition metals of interest in this study, especially considering the lack of an alkoxide feed stock (e.g., Na-ethoxide) for metathesis reactions.

3. Provisional passivation by chloride. On exposure to aqueous HCl, alloy samples react with it corresponding to typical corrosion reactions, leading to the dissolution of metal ions and the formation of hydrogen gas:



However, it is also energetically favorable to form a metal chloride, especially as the sample is removed from the solution with residual HCl adsorbed on the surface. This would lead to a metal-(Fe-, Cr-, Ni-) chloride layer on the alloy surface, which could have multiple impacts on the efficacy of the process. If the surface layer is adherent and covers the majority of the sample surface, the chloride, as such, may act as a provisional passivating layer. Binding the Cr at the alloy surface to Cl, so it is not available to form Cr oxide when exposed to ambient oxygen later, effectively inhibits formation of the regular, Cr-oxide-rich passivating oxide layer, which (presumably) poses the strongest barrier to carbon infusion.

The resulting condition of the alloy surface in C₂H₅OH depends on the solubility of the hypothetical Cr chlorides. Table 2 classifies the solubility of various Fe, Cr, and Ni chlorides [42–46]. The most common modification of chromic chloride, CrCl₃, is hexahydrate. It is soluble in both water and C₂H₅OH. Another important modification is anhydrous CrCl₃, which, in pure form, is mostly insoluble in both water and C₂H₅OH. However, if traces of CrCl₂ (or another reduction agent) are present, this can catalyze dissolution in H₂O, which is strongly exothermic [47].

Table 2. Chloride solubility in ethanol.

Compound	Soluble in H ₂ O	Soluble in Ethanol	Reference
CrCl ₃ Anhydrous	If Catalyzed	No	[42,47]
CrCl ₃ Hexahydrate	Yes	Yes	[42]
CrCl ₂	Very	No	[43]
Fe ₃ Cl	Very	Very	[44]
Fe ₂ Cl	Very	Yes	[45]
Ni ₂ Cl	Very	Yes	[46]

If the hypothetical provisional passivating layer mainly consisted of the hexahydrate modification of CrCl₃, it would be less susceptible to which rinsing agent is used [42]. Since in our process samples rinsed in ethanol performed considerably better than samples rinsed in water, the provisional passivating layer much more likely consisted of chlorides that are soluble in water, but insoluble in C₂H₅OH. The only chlorides matching this requirement are chromium dichloride (chromous chloride), CrCl₂, and the anhydrous modification of CrCl₃. So, if an alloy part covered with (Fe, Cr, Ni) chlorides were rinsed in cold water, and at least traces of CrCl₂ were present, all chlorides would be removed. Rinsing in C₂H₅OH, in contrast, would remove all chlorides except CrCl₃ and CrCl₂. Thus, the observation that the process works with rinsing in C₂H₅OH, but not with rinsing in H₂O, indicates that the critical compounds that need to form to generate a chloride-based provisional passivating layer are CrCl₂ or anhydrous CrCl₃. Thermodynamic data for similar conditions [48] indicate that the Gibbs energy of formation is lower for CrCl₂ than for CrCl₃. Cr and HCl readily form CrCl₂, while forming CrCl₃ from CrCl₂ usually requires significant activity of oxygen (2CrCl₂ + 1/2O₂ + 2HCl → 2CrCl₃ + H₂O). Accordingly, the provisional passivating layer most likely consists of CrCl₂. While the low-temperature carburization temperature is significantly below the melting temperatures of chlorides, the thin layers considered here may be removed by sublimation [49] or via reduction by the H₂ in the low-temperature carburization gas mixture.

5. Conclusions

1. For effective low-temperature carburization of Cr-containing alloys, it is essential to properly activate the surface. A severely plastically deformed, highly dislocated and/or nanograined Beilby layer, e.g., generated by surface machining, does not enhance carbon transport by “pipe” diffusion, but constitutes a diffusion barrier to carbon.
2. Therefore, surface activation for low-temperature carburization should include removal of the passivating oxide layer and removal of the Beilby layer.
3. For AISI-AL-6XN, C₂H₂ (acetylene) performs well as carburizing gas at a low temperature (723 K). It is effective at removing the passivating oxide layer, but does not etch the metal and, thus, cannot aid in removing the Beilby layer.
4. Effective surface activation for low-temperature carburization of AISI-AL-6XN or similar alloys, especially with C₂H₂ as carburizing gas, can be performed outside of the carburization furnace by etching in aqueous (liquid) HCl, followed by rinsing in C₂H₅OH and drying in nitrogen. Instead of the Cr-rich passivating oxide layer that usually forms on these alloys, this procedure generates a provisional passivating layer, which is readily removed upon heating and exposing the alloy to the carburizing gas mixture.
5. Among three alternatives considered for the nature of the provisional passivating layer, the most likely mechanism is surface coverage by chlorides that are insoluble in ethanol.
6. External activation by etching with concentrated aqueous HCl is more efficient and causes less damage to furnace hardware than the current industrial practice of activation by hot gaseous HCl within the carburization furnace.

Author Contributions: Conceptualization: F.E., A.H.H., Z.L. Experimental work: Z.L. Methodology: Z.L., F.E. Software: F.E. Chemical and thermodynamic analysis: C.I. Theory, modeling: F.E., C.I., A.H.H. Writing—original draft preparation: Z.L. Writing—review and editing: F.E. Technical manuscript preparation: F.E. Visualization: F.E. Supervision: F.E. Project administration: F.E. Funding acquisition: F.E., A.H.H.

Funding: We acknowledge financial support for the research project 12-3451 from the DOE-NEUP program under contract number 00128081.

Acknowledgments: We appreciate the discussions with H. Kahn, S. Collins, P. Williams, and S. Marx and thank the engineers of the Swagelok Center for Surface Analysis of Materials at Case Western Reserve University for their assistance.

Conflicts of Interest: The authors declare no conflict of interest.

References

1. Grabke, H.; Wolf, I. Carburization and oxidation. *Mater. Sci. Eng.* **1987**, *87*, 23–33. [[CrossRef](#)]
2. Yin, R. Carburization of 310 stainless steel exposed at 800–1100 °C in 2% CH₄/H₂ gas mixture. *Corros. Sci.* **2005**, *47*, 1896–1910. [[CrossRef](#)]
3. Michal, G.M.; Gu, X.; Jennings, W.D.; Kahn, H.; Ernst, F.; Heuer, A.H. Paraequilibrium Carburization of Duplex and Ferritic Stainless Steels. *Metallurg. Mater. Trans.* **2009**, *40*, 1781–1790. [[CrossRef](#)]
4. Collins, S.R.; Williams, P.C.; Marx, S.V.; Heuer, A.H.; Ernst, F.; Kahn, H. Low-Temperature Carburization of Austenitic Stainless Steels. In *ASM Handbook, Volume 4D: Heat Treating of Irons and Steels*; Dossett, J., Totten, G., Eds.; ASM International: Materials Park, OH, USA, 2014; Volume 4, pp. 451–460.
5. O’Donnel, L.; Michal, G.M.; Ernst, F.; Kahn, H.; Heuer, A.H. Wear Maps for Low Temperature Carburized 316L Austenitic Stainless Steel Sliding Against Alumina. *Surf. Eng.* **2010**, *26*, 284–292. [[CrossRef](#)]
6. Agarwal, N.; Kahn, H.; Avishai, A.; Michal, G.; Ernst, F.; Heuer, A.H. Enhanced Fatigue Resistance in 316L Austenitic Stainless Steel Due to Low-Temperature Paraequilibrium Carburization. *Acta Mater.* **2007**, *55*, 5572–5580. [[CrossRef](#)]
7. Martin, F.J.; Lemieux, E.J.; Newbauer, T.M.; Bayles, R.A.; Natishan, P.M.; Kahn, H.; Michal, G.M.; Ernst, F.; Heuer, A.H. Carburization-Induced Passivity of 316L Austenitic Stainless Steel. *Electrochem. Solid State Lett. C* **2007**, *10*, 76–78. [[CrossRef](#)]

8. Martin, F.; Natishan, P.; Lemieux, E.; Newbauer, T.; Rayne, R.; Bayles, R.; Kahn, H.; Michal, G.; Ernst, F.; Heuer, A. Enhanced corrosion resistance of stainless steel carburized at low temperature. *Metallurg. Mater. Trans. A* **2009**, *40*, 1805–1810. [[CrossRef](#)]
9. Niu, W.; Li, Z.; Ernst, F.; Lillard, R.S. Properties of the Passive Film Formed on Interstitially Hardened AISI 316L Stainless Steel. *Electrochim. Acta* **2015**, *176*, 410–419. [[CrossRef](#)]
10. Williams, P.; Collins, S. Mechanical design using low-temperature carburization. *JOM* **2008**, *60*, 27–30. [[CrossRef](#)]
11. Heuer, A.H.; Ernst, F.; Kahn, H.; Collins, S.R.; Natishan, P.M. Case Hardening of Corrosion Resistant Alloys: Low-Temperature Carburization and “Colossal” Interstitial Supersaturation. In *Encyclopedia of Iron, Steel, and Their Alloys*; Totten, G., Colas, R., Eds.; Taylor and Francis: London, UK, 2016.
12. Nomura, K.; Ujihira, Y. Analysis of oxide layers on stainless steel (304, and 316) by conversion electron Mössbauer spectrometry. *J. Mater. Sci.* **1990**, *25*, 1745–1750. [[CrossRef](#)]
13. Finch, G.I.; Quarrell, A.G. The Beilby Layer. *Nature* **1936**, *137*, 516. [[CrossRef](#)]
14. Ge, Y.; Ernst, F.; Kahn, H.; Heuer, A.H. The Effect of Surface Finish on Low-Temperature Acetylene-Based Carburization of 316L Austenitic Stainless Steel. *Metallurg. Mater. Trans. B* **2014**, *45*, 2338–2345. [[CrossRef](#)]
15. Ge, Y. Acetylene-Based Carburization and Nitrocarburizing of 316L Austenitic Stainless Steel. Ph.D. Thesis, Case Western Reserve University, Cleveland, OH, USA, 2013.
16. Nemat-Nasser, S.; Guo, W.G.; Kihl, D.P. Thermomechanical response of AL-6XN stainless steel over a wide range of strain rates and temperatures. *J. Mech. Phys. Solids* **2001**, *49*, 1823–1846. [[CrossRef](#)]
17. Li, Z. Surface Hardening of Austenitic Fe–Cr–Ni Alloys for Accident-Tolerant Nuclear Fuel Cladding. Ph.D. Thesis, Case Western Reserve University, Cleveland, OH, USA, 2018.
18. Gentil, J. Surface Modification of Superaustenitic and Maraging Stainless Steels by Low-Temperature Gas-Phase Carburization. Ph.D. Thesis, Case Western Reserve University, Cleveland, OH, USA, 2008.
19. Ernst, F. Background of SAM Atom-Fraction Profiles. *Mater. Charact.* **2017**, *125*, 142–151. [[CrossRef](#)]
20. Ernst, F.; Cao, Y.; Michal, G.M. Carbides in Low-Temperature Carburized Stainless Steels. *Acta Mater.* **2004**, *52*, 1469–1477. [[CrossRef](#)]
21. Ernst, F.; Avishai, A.; Kahn, H.; Gu, X.; Michal, G.M.; Heuer, A.H. Enhanced Carbon Diffusion in Austenitic Stainless Steel Carburized at Low Temperature. *Metallurg. Mater. Trans. A* **2009**, *40*, 1768–1780. [[CrossRef](#)]
22. Christiansen, T.; Hummelshøj, T.S.; Somers, M.A. Gaseous carburising of self-passivating Fe–Cr–Ni alloys in acetylene–hydrogen mixtures. *Surf. Eng.* **2011**, *27*, 602–608. [[CrossRef](#)]
23. Ishii, A.; Li, J.; Ogata, S. “Conjugate Channeling” Effect in Dislocation Core Diffusion: Carbon Transport in Dislocated BCC Iron. *PLoS ONE* **2013**, *8*, e60586. [[CrossRef](#)] [[PubMed](#)]
24. Cottrell, A.H.; Bilby, B.A. Dislocation Theory of Yielding and Strain Ageing of Iron. *Proc. Phys. Soc. Sect. A* **1949**, *62*, 49. [[CrossRef](#)]
25. Veiga, R.G.A.; Perez, M.; Becquart, C.S.; Domain, C.; Garruchet, S. Effect of the stress field of an edge dislocation on carbon diffusion in α -iron: Coupling molecular statics and atomistic kinetic Monte Carlo. *Phys. Rev. B* **2010**, *82*, 054103. [[CrossRef](#)]
26. Christiansen, T.; Somers, M.A. Determination of concentration dependent diffusion coefficient of nitrogen in expanded austenite. *Int. J. Mater. Res.* **2008**, *24*, 159–167. [[CrossRef](#)]
27. Higashi, G.; Chabal, Y.; Trucks, G.; Raghavachari, K. Ideal hydrogen termination of the Si(111) surface. *Appl. Phys. Lett.* **1990**, *56*, 656–658. [[CrossRef](#)]
28. Allongue, P.; De Villeneuve, C.H.; Pinson, J.; Ozanam, F.; Chazalviel, J.; Wallart, X. Organic monolayers on Si(111) by electrochemical method. *Electrochim. Acta* **1998**, *43*, 2791–2798. [[CrossRef](#)]
29. Li, Z.; Ernst, F.; Kahn, H.; Heuer, A. Alloy Surface Activation by Immersion in Aqueous Acid Solution. U.S. Patent Application, 15/308,223, 23 March 2017.
30. Battino, R.; Rettich, T.R.; Tominaga, T. The Solubility of Oxygen and Ozone in Liquids. *J. Phys. Chem. Ref. Data* **1983**, *12*, 163–178. [[CrossRef](#)]
31. Schumpe, A.; Luehring, P. Oxygen diffusivities in organic liquids at 293.2 K. *J. Chem. Eng. Data* **1990**, *35*, 24–25. [[CrossRef](#)]
32. Lin, C.; Al-Muhtaseb, S.A.; Ritter, J.A. Thermal treatment of sol-gel derived nickel oxide xerogels. *J. Sol-Gel Sci. Technol.* **2003**, *28*, 133–141. [[CrossRef](#)]
33. Brown, D.A.; Cunningham, D.; Glass, W. Studies of chromium(III) alkoxides. *J. Chem. Soc. A Inorg. Phys. Theor.* **1968**, 1563–1568. [[CrossRef](#)]

34. Holec, P.; Plocek, J.; Nižňanský, D.; Vejpravova, J.P. Preparation of MgFe₂O₄ nanoparticles by microemulsion method and their characterization. *J. Sol-Gel Sci. Technol.* **2009**, *51*, 301–305. [[CrossRef](#)]
35. Williams, P.C.; Marx, S.V. Low Temperature Case Hardening Processes. U.S. Patent 6,093,303, 25 July 2000.
36. Kessler, V. Alkoxides and Alkoxosynthesis. In *Comprehensive Inorganic Chemistry II*; Elsevier: Amsterdam, The Netherlands, 2013; pp. 455–470. [[CrossRef](#)]
37. Bryndza, H.E.; Tam, W. Monomeric metal hydroxides, alkoxides, and amides of the late transition metals: synthesis, reactions, and thermochemistry. *Chem. Rev.* **1988**, *88*, 1163–1188. [[CrossRef](#)]
38. Edema, J.J.H.; Gambarotta, S.; Van Bolhuis, F.; Spek, A.L. Chromium(II) Alkoxides: Synthesis and Crystal Structure of the Monomeric [(RO)₄Cr][Na(TMEDA)]₂ (R = 2,6-dimethylphenyl) and dimeric [(RO)₈Cr₂][NaL]₄ (R = phenyl; L = THF, pyridine) Without a Chromium–Chromium Bond. An Insight Into the Question of Chromium–Chromium Quadruple Bond Formation. *J. Am. Chem. Soc.* **1989**, *111*, 2142–2147. [[CrossRef](#)]
39. Seisenbaeva, G.A.; Gohil, S.; Suslova, E.V.; Rogova, T.V.; Turova, N.Y.; Kessler, V.G. The synthesis of iron(III) ethoxide revisited: Characterization of the metathesis products of iron(III) halides and sodium ethoxide. *Inorg. Chim. Acta* **2005**, *358*, 3506–3512. [[CrossRef](#)]
40. Mehrotra, R. Synthesis and Reactions of Metal Alkoxides. *J. Non-Cryst. Solids* **1988**, *100*, 1–15. [[CrossRef](#)]
41. Mehrotra, R.; Mahendra, K. Synthesis and characterization of some chloride alkoxides of chromium(III) and their addition complexes. *Inorg. Chim. Acta* **1984**, *81*, 163–167. [[CrossRef](#)]
42. Santonen, T.; Organization, W.H. *Inorganic Chromium(III) Compounds*; World Health Organization: Geneva, Switzerland, 2009.
43. Lewis, R.J. *Hawley's Condensed Chemical Dictionary*, 15th ed.; John Wiley & Sons: Hoboken, NJ, USA, 2007.
44. Company, C.R.; Weast, R.C.; Astle, M.J.; Beyer, W.H. (Eds.) *CRC Handbook of Chemistry and Physics: A Ready-Reference Book of Chemical and Physical Data*; CRC Press: Boca Raton, FL, USA, 1988.
45. Budavari, S. (Ed.) *The Merck Index: An Encyclopedia of Chemicals, Drugs, and Biologicals*, 11th ed.; Merck: Rahway, NJ, USA, 1989.
46. Prager, J.C. *Environmental Contaminant Reference Databook*; Van Nostrand Reinhold: New York, NY, USA, 1995.
47. Riedel, E.; Janiak, C. *Anorganische Chemie*; de Gruyter: Berlin, Germany, 2011; Chapter 5.14, p. 813.
48. Illing, C. Chemical Mechanisms and Microstructural Modification of Alloy Surface Activation for Low-Temperature Carburization. Master's Thesis, Case Western Reserve University, Cleveland, OH, USA, 2018.
49. Titov, V.A.; Grinberg, E.E. The thermodynamic characteristics of sublimation of chromium trichloride. *Russ. J. Phys. Chem.* **2006**, *80*, 689–692. [[CrossRef](#)]



© 2018 by the authors. Licensee MDPI, Basel, Switzerland. This article is an open access article distributed under the terms and conditions of the Creative Commons Attribution (CC BY) license (<http://creativecommons.org/licenses/by/4.0/>).